Applied Water Science (2019) 9:159
https://doi.org/10.1007/s13201-019-1039-0

ORIGINAL ARTICLE

Removal of organic pollutant (pyrene) from aqueous solution using coordination polymer of $[Cu(Pic)_2(H_2O)_2]\cdot H_2O$ (CP-1) as adsorbent

Adedibu C. Tella[1] · Margaret D. Olawale[1,2] · Joshua A. Obaleye[1] · Vincent O. Adimula[1] · Lukman O. Alimi[3] · Peter A. Ajibade[4]

Received: 19 June 2019 / Accepted: 16 September 2019

Abstract

Adsorptive removal of organic pollutant (pyrene) was carried out using coordination polymer $[Cu(Pic)_2(H_2O)_2]\cdot H_2O$ (CP-1) (where "Pic" represents picolinic acid), which was prepared from copper acetate monohydrate and picolinic acid. The compound was characterized by spectroscopic techniques, SEM, elemental and thermal analyses and X-ray crystallographic analysis. The crystal structure of CP-1 shows a centrosymmetric triclinic space group P-1 in which $a = 5.0924$ (4) Å, $b = 7.5172$ (6) Å, $c = 9.0965$ (8) Å. The Cu^{2+} ion is seen to have an octahedral geometry, which is bonded to oxygen atoms from the picolinic acid and nitrogen atoms from the pyridine rings. Pyrene adsorption from aqueous media was studied with the prepared adsorbent (CP-1). The kinetic model was observed to be second order, and the sorption data fitted best into the Langmuir model. The absorbent, CP-1, was shown to have a 90.91 mg/g adsorption capacity (maximum) for pyrene in this study at 25 °C. Compound CP-1 can thus be presented as a potential adsorbent in the treatment of pyrene-polluted water.

Keywords Picolinate · X-ray crystallography · Pyrene · Adsorption · Isotherms

Introduction

Toxic organic substances, such as the polynuclear/polycyclic aromatic hydrocarbons (PAHs), consist of several chemicals made up of varying quantities of carbon and hydrogen atoms joined in a ring-like manner and formed fused aromatic rings (Baek et al. 1999). PAHs range in appearance from colorless to colored (white, pale yellow, or green). They exhibit reduced solubility in the aqueous medium while being very lipophilic. Several of these are known to have reduced vapor pressure, when present in the atmosphere, which favors their adsorption on particles. They can also experience photodecomposition, especially on exposure to ultraviolet light from solar energy (Baek et al. 1999; Byeong-Kyu and Van-Tuan 2010), and are generated predominantly by incomplete pyrolysis procedures involving coal, natural gas, crude oil, waste, vehicle exhaust pipe as well as in normal carbonization (Jernelöv 2010; Nriagu 2011).

PAHs have been reportedly detected, severally, in environmental media and food. Obviously, they can also originate as emissions from volcanoes and forest fires (Byeong-Kyu and Van-Tuan 2010; Ravindra et al. 2006). Investigations have confirmed that breathe exposure to these toxic substances can result in lung cancer. A study of diseases associated with PAHs, using aluminum processing and coke-oven plant workers, gave evidence of inhalation of these substances, and most of them are known to be affected with lung cancer leading to excessive mortality. The growths in lung cancer cases of coke-oven workers relate closely with the working period used while working with the coke oven with an average benzo[a]pyrene concentration of about 30 mg/m^3 (Hemminki 1993; Donata 2011). Polycyclic aromatic hydrocarbons are majorly classified into two based on

Electronic supplementary material The online version of this article (https://doi.org/10.1007/s13201-019-1039-0) contains supplementary material, which is available to authorized users.

✉ Adedibu C. Tella
ac_tella@yahoo.co.uk; adedibu@unilorin.edu.ng

[1] Department of Chemistry, P.M.B.1515, University of Ilorin, Ilorin, Kwara State, Nigeria

[2] Department of Physical and Chemical Sciences, Elizade University, Ilara-Mokin, Ondo State, Nigeria

[3] Department of Chemistry and Polymer Science, Stellenbosch University, Stellenbosch, Western Cape 7602, South Africa

[4] School of Chemistry and Physics, University of KwaZulu- Natal, Private Bag X01, Scottsville, Pietermaritzburg 3209, South Africa

Published online: 24 September 2019

molecular weight, namely the mobile and non-mobile PAHs. Of chief environmental disquiet among these are those capable of being dispersed with varying molecular weight (128.16–300.36 g/mol), while higher molecular weights (beyond that of coronene) are rather less dispersed because of their large molecule sizes, bulkiness, reduced volatility and solubility (Zhu et al. 2009). Thousands of these dispersible PAHs have structural difference based on the location of their aromatic rings and the number thereof, as well as the position of some substituents present on the main ring structure. Those that are unsubstituted, with low molecular weights, having 2 or 3 ring structures, are reported for their acute toxicity to some organisms. Such compounds include naphthalenes, fluorenes, phenanthrenes, pyrene and anthracenes, which are known to be carcinogenic, cocarcinogenic, and tumor producers, whereas those of higher molecular weights (4–7 ring aromatics) mostly do not impose a threat to the environment and aquatic lives (Ali et al. 2012; Liu et al. 2008; Chen et al. 2004; Lee and Grant 1981; Cooke and Dennis 1984).

Coordination polymers are novel (sometimes crystalline and microporous) covalent compounds, exhibiting tunable properties, framework suppleness, huge surface areas, catalytic activities (Lee et al. 2009) and adsorption purposes (Mueller et al. 2006; Tella and Aaron 2012; Tella et al. 2017a, b). These distinct chemical and physical properties make them a field rapidly progressing in material science (Mueller et al. 2006; Tella and Aaron 2012; Tella et al. 2017a, b). Coordination polymers are formed via metals (or metal cluster) and bridging ligand covalent linkages. The optimal choice of metal and linker has substantial effects on the structure and properties of these solids formed (Alhamami et al. 2014; Dey et al. 2013; Lee et al. 2013; Zhao et al. 2016). In continuation of our studies on the application of some coordination polymers in environmental remediation (Tella et al. 2014, 2017a, b, 2018), we hereby report the preparation of a crystalline Cu^{2+} picolinate coordination polymer, presented as CP-1, for the removal of pyrene from aqueous medium. There has been no prior report of usage of the prepared compound CP-1, as a material for adsorption of pyrene.

Experimental section

Materials and physical measurements

Picolinic acid, copper(II) acetate and all solvents used were bought from Sigma-Aldrich Co., Germany, and used as obtained without additional purification. The melting point was taken on a WRS-1B melting point apparatus. Elemental analysis was performed with a series II PerkinElmer CHN Analyzer 2400. The infrared data were collected with FTIR 8400 s Spectrophotometer (SHIMADZU scientific model). Thermal analysis was done on a TGA Q500 V20.13. Diffraction patterns were obtained from a Bruker D8 Advance diffractometer (CuKα radiation; $\lambda = 1.5406$ Å) generating X-rays from a 30-kV source and a 40-mA current. Crystallographic data were measured with a Nonius Kappa CCD diffractometer and graphite-monochromated M_oK radiation. A direct method of structure elucidation was used and F^2 refinement carried out. Hot-stage microscope was used to study the behavioral pattern of the crystal under heat.

Synthesis of CP-1

Picolinic acid (1 mmol, 0.123 g) was dissolved in 10 mL acetone, and $Cu(CH_3COO)_2{\cdot}H_2O$ (0.5 mmol, 0.101 g) was dissolved in 10 mL methanol. The two solutions were mixed together, and 0.2 mL triethylamine was added. This mixture was continuously stirred and refluxed for 30 min at 200 °C. Thereafter, the solution was kept at room temperature to evaporate slowly, and blue colored crystals were formed and isolated from the solution after 9 days, washed with acetone: methanol (1:1) mixture and placed in a desiccator. The reaction equation is illustrated in Scheme 1.

Procedure for the adsorptive removal of pyrene

The pyrene stock standard of 200 ppm was prepared: 200 mg of pyrene (molecular formula: $C_{16}H_{10}$; molecular weight: 202.3 g/mol) in 1 liter of acetone. From the stock solution of pyrene, different working standards (5–30 ppm) were prepared by serial dilution with acetone. The solutions were analyzed for the PAHs using UV–visible spectrophotometer (Shimada UV spectrophotometer, UV-1800) by monitoring the absorbance changes at λ_{max} 351 nm for pyrene solutions, and the calibration curve was plotted.

Prior to adsorption, the compound CP-1 was dried for 3 h at 110 °C; thereafter, it was left to cool in a desiccator. The activated adsorbent (compound CP-1) was weighed (0.01 g) into a 30-ml pyrene solution, and the adsorption process was carried out using an orbital shaker at 200 revolutions per minute (rpm) for a fixed time (10–300 min) at 25 °C. A portion of the solution was taken after every 30 min for UV–Vis analysis. The amount of pyrene removed from the solution by the adsorbent was obtained by a mass–balance relationship.

Results and discussion

The melting point of CP-1 was higher than that of the ligand as shown in Table S1 suggesting the formation of the CP-1. Spectra data from the infrared and ultraviolet visible spectroscopic analysis of CP-1 differ from the picolinic acid spectra, indicating a successful coordination of the ligand to the metal

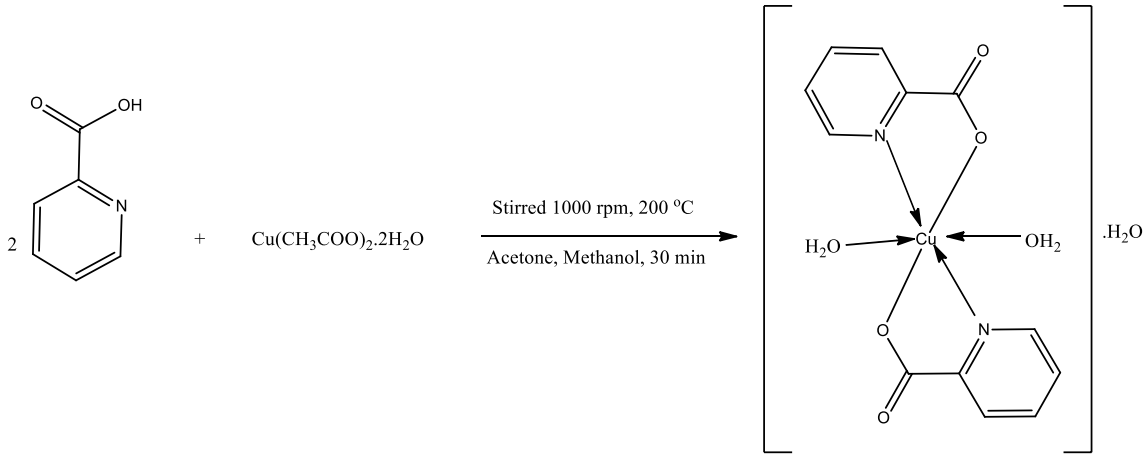

Scheme 1 Synthesis of CP-1. Yield: 76%, M. wt = 343.78 g/mol, M. pt = 215 °C, Analc. Found (Calcd) % for $[C_{12}H_{10}N_2O_6Cu]$: C, 41.83 (41.89); H, 3.47 (3.49); N, 8.11 (8.14), IR (KBr, cm^{-1}): 1369, 1896, 1045, 1598, 547, 457. UV–Vis (DMSO) nm: 210, 219, 548.

ion. The data showed a strict 1:2 composition (metal: picolinic acid) with the absence of acetate. The elemental analysis results agreed with the formula $[C_{12}H_{10}N_2O_6Cu]$. The molecular structure of CP-1 was confirmed by X-ray crystallography.

FTIR spectra of picolinic acid and CP-1

The observed picolinic acid IR band frequencies and that of CP-1 are represented in Table S2. It can be seen from the table that the relevant stretching frequencies in the coordination polymer shifted in comparison with that of the ligand.

The free picolinic acid showed a broadband at 3111 cm^{-1} as a result of the ν(O–H) present. This was shifted to 3076 cm^{-1} in CP-1 (Cu(II) picolinate), 3086 cm^{-1} in the Cd(II) picolinate (Tella et al. 2017a, b), MOF and 3163 cm^{-1} in the Ni(II) picolinate (Tella et al. 2017a, b). This indicates the deprotonated form of the ν(O–H) group in 1. Shifts in the absorption bands of ν(C=N) in 1 are ascribed to the coordination of the picolinate ion to the metal atom through the pyridine group making the picolinate ion bidentate and a bridging moiety (Antolini et al. 1982).

Electronic spectra of picolinic acid and CP-1

The UV–Vis analysis (Table S3) of CP-1 with that of picolinic acid shows that the picolinic acid is bonded with the central metal ion with the appearance of peaks that indicate the ^2E_g-to-$^2T_{2g}$ transitions in 1. UV–Vis spectrum of the ligand shows bands at 244 nm and 379 nm due to the $\pi-\pi^*$ and $n-\pi^*$ transitions, respectively, revealing the presence of C=C and C=O bonds. UV–Vis spectrum of CP-1 shows absorption at 210 nm and 219 nm assigned to the transitions of $\pi-\pi^*$ and $n-\pi^*$, respectively. These bands confirm the presence of C=C and C=O bonds within the complex form. Electronic transition from ^2E_g to $^2T_{2g}$ vividly shows copper as the metal that bonded to the picolinic acid.

X-ray crystallographic analysis of CP-1

The ORTEP structure of CP-1 showing all atoms and numbering is shown in Fig. 1. Crystal data summary, selected bond angles and lengths of CP-1 are given in Tables 1, 2 and 3. The compound crystallizes in the P-1 space group. Crystallographic data of the complex revealed the copper ion is polymerically almost in a conventional octahedral fashion with twofold picolinate ions bonded on side way of each of

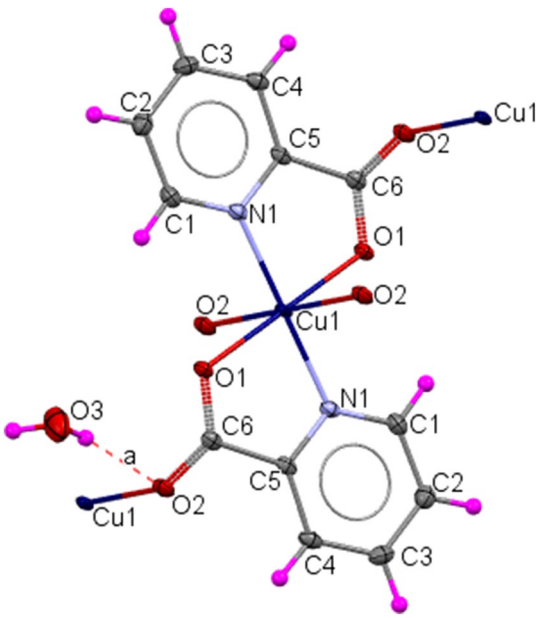

Fig. 1 Thermal ellipsoid plot (ORTEP) view of CP-1 showing all atoms and numbering

copper metal ions. The two equatorial carboxylate oxygen atoms bonded to copper that directly bond to the pyridine displayed a Cu–O bond length average of 1.947 Å, comparing favorably with the range 1.930–1.990 Å (Tella et al. 2018) usually observed for copper complexes. The Cu–O bond length 2.697 Å observed in the other two axial oxygen atoms on copper metal is elongated in length representing the *Jahn–Teller* distortion effect (Jahn and Teller 1937). The two Cu–N bonds gave bond length of 1.962 Å which concurred favorably with expected range of 1.974–2.008 Å (Shriver and Atkins 1999) usually observed for copper complexes.

The complex exhibits an octahedral geometry in which the copper ion is bonded with one copper ion which is bonded with four oxygen atoms of picolinic acid and two nitrogen atoms from the pyridine of the picolinic acid through dative bonding. One molecule of water, acting as solvent of crystallization, is found outside the lattice linked via hydrogen bonding from the carboxylate oxygen which acts as electron donor to the water molecule.

Geometric distortion of a nonlinear molecular system is well observed in the octahedral coordination scheme of 1 where the two Cu–O equatorial bonds are significantly shorter, while the two Cu–O axial bonds are longer displaying Jahn–Teller distortion effect (Shriver and Atkins 1999), a phenomenon commonly encountered in a six-coordinate Cu^{2+} compound (Schlichte et al. 2004). In the Cu^{2+} complex, three electrons transit into the two degenerate e_g orbitals leading to an observed distortion of one of the molecular axes. Occurrence of this distortion can be seen in elongation or occasional shortening of bonds along the fourfold axis.

Table 1 Crystal structural data of CP-1

Identification cypher	CP-1
Empirical formula	$C_{12}H_8CuN_2O_4{\cdot}2(OH_2)$
Formula weight	343.78
Crystal system	Triclinic
Space group	-P1
Crystal shape/color	Plate/blue
Unit cell dimensions	$a=5.0924$ (4) Å
	$b=7.5172$ (6) Å
	$c=9.0965$ (8) Å
	$\alpha=75.888$ (3)°
	$\beta=85.109$ (3)°
	$\gamma=72.255$ (3)°
Cell volume (Å^3)	321.62 (3) Å^3
Z value	1
Density (calculated) (g cm^{-3})	$D_x=1.775$ Mg m^{-3}
F(000)	175
Θ range for data collection	$\theta=5°$–$69°$
CuKα radiation	$\lambda=1.54178$ Å
Crystal size: min, mid, max	0.15×0.13×0.03 mm

Table 2 Selected bond distances (Å) and angles (°) for CP-1

Bond length (Å)		Bond angles (°)	
Cu1–O1	1.9475 (11)	O2^{i}–Cu1–O2^{ii}	179.996
Cu1– O2	2.6965 (12)	N1–Cu1–O1	83.85 (5)
Cu1–N1	1.9618 (14)	O1^{i}–Cu1–O1^{ii}	179.994
		O2^{i}–Cu1–N1^{ii}	90.72 (5)
		O1^{iii}–Cu1–N1^{ii}	96.15 (5)

The geometrical parameters for the crystal complex agree with the previously published work on similar compounds containing Cu^{2+} in an octahedral geometry with oxygen and nitrogen donor atoms (Jahn and Teller 1937).

The crystal packing is depicted in Fig. 2. The packing of the CP-1 consists of chains, mutually interacting through the hydrogen bonding, thereby stabilizing the crystal structure as shown in Fig. 3.

The structure of the compound is fascinating due to its polymeric nature (Fig. 4) because the copper central metal is linked with two symmetries of equivalent picolinate ion which in turn can also be coordinated to another copper ion through its oxygens, thereby resulting in the formation of giant polymeric crystal structure. The linking is achieved by hydrogen bonding of the type C–H···O (Table 3) and assisted by some measure of π-stacking of picolinate ring.

The H_2O molecule present in the structure of 1 was observed to be connected to the lattice through inter-molecular hydrogen bond (O–H···O) as detailed in Table 3 predicting the stability of 1.

Thermal characterization of CP-1

A weight of 4.4 mg of the CP-1 was taken and thermally studied using TGA Q500 in an oxygen dynamic atmosphere (10 °C/min; 50 mL/min). Figure 5 reveals the thermal decomposition patterns of this crystal showing the first decomposition step with a percentage weight loss of 3.49% (5.23%) (experi. (calc.)) corresponding to the loss of molecule of lattice H_2O at about 90 °C. The second stage of the decomposition is due to loss of coordinated water at 255 °C with percentage weight

Table 3 Intermolecular interaction distances (Å) for CP-1

D—H···*A*	Symm	*D*—H	H···*A*	*D*···*A*	*D*—H···*A*
C4–H41···O2	$-x+4$, $-y-1$, $-z+1$	0.94	2.38	3.203 (2)	147 (1)
O3–H1···O2	–	0.82	2.09	2.903 (2)	170 (3)
O3–H2···O3	$-x+4$, $-y$, $-z$	0.78	2.05	2.800 (2)	161 (4)

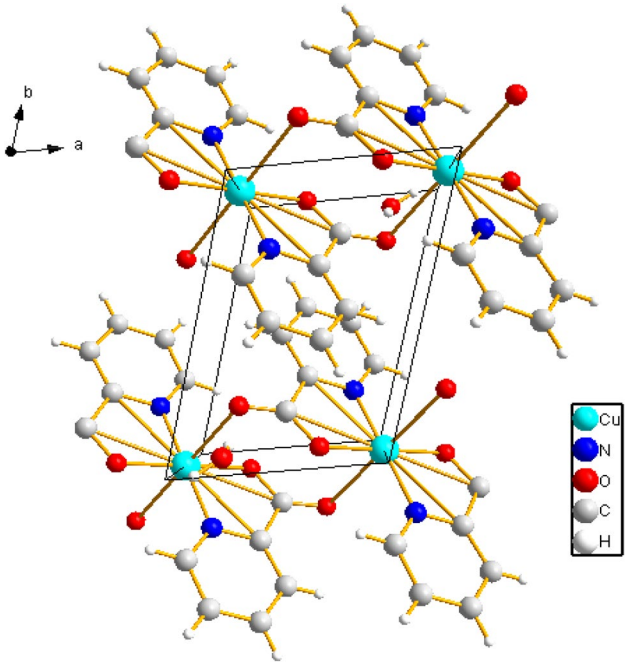

Fig. 2 Crystal packing of CP-1

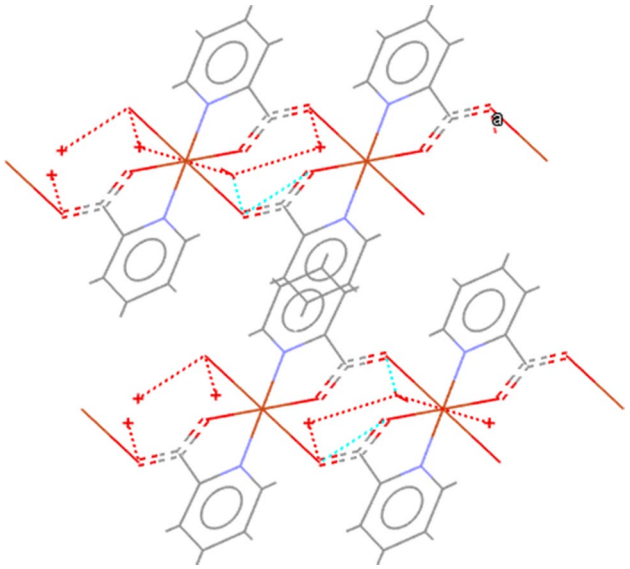

Fig. 3 Hydrogen bonding in compound CP-1

loss of 5.77% (5.23%) (experi. (calc.)). The third stage of decomposition between 275 and 310 °C is attributed to gradual decomposition of the ligand picolinate and remaining coordinated water with percentage weight loss of 45.39% (45.95%) (experi. (calc.)). The DTG curve of the $[Cu(Pic)_2(H_2O)_2]\cdot H_2O$ shows T_{DTG} peaks at temperatures of 90 °C, 255 °C, and 310 °C, corresponding to the decomposition temperatures observed in the TGA curve. The strong T_{DTG} peak observed at 310 °C compliments the observed organic picolinate backbone decomposition observed in the TGA curve.

Hot-stage microscope examination of compound CP-1

The hot-stage microscopy was carried out to facilitate the understanding of the thermal behavior of CP-1. The crystal was gradually heated from room temperature to 500 °C to visualize how the guest molecule leaves the system under microscope (Fig. 6a–d). Slight color change can be observed as the crystal is heated gradually accompanied by loss of solvent molecules and organic species. Hot-stage microscopy revealed the loss of optical transparency in the crystal on heating from R.T to 400 °C. Figure 6b reveals the loss of the lattice water molecule at 90 °C and coordinated water around 255 °C (Fig. 6c) and decomposition of the organic ligand picolinate at 310 °C (Fig. 6d) which also agrees with TGA results. The crystals change from blue to opaque after 310 °C.

Powder X-ray diffraction studies of CP-1

The powder X-ray diffraction patterns of the 1 are shown in Fig. 7. The observed pattern from 1 was compared with calculated pattern from the crystal structure data. It can be seen that PXRD patterns of the 1 agree well with the simulated pattern, indicating that the products have been successfully obtained as crystalline phase.

Adsorption study of pyrene on CP-1

Physicochemical considerations (i.e., concentration of adsorbate, dosage, time of contact, temperature and pH effects) were included for a determination of the adsorption efficacy. Mass–balance relationship was then used to compute the quantity of pyrene adsorbed onto CP-1 according to the below:

$$q_e = \left(C_0 - C_e\right)V/W$$

C_0 and C_e (mg/L) are the concentrations at time 0 and t, respectively; V = vol. used (dm^3); W, weight (g) of the adsorbents, respectively.

The various pHs of the pyrene solutions determination were attained using 0.1 M HCl or 0.1 M NaOH solutions and monitored using a pH meter. The initial concentrations of PAHs were 5–30 ppm.

Effect of initial concentration

The amount of pyrene adsorbed (Figure S1) on CP-1 increased as the concentration of the adsorbate increased

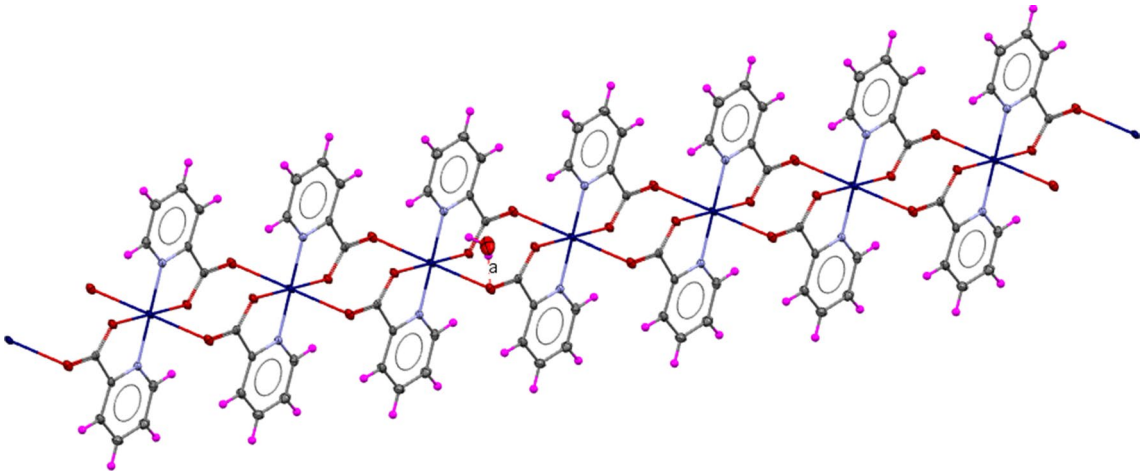

Fig. 4 Extended view of CP-1 showing 1D grid polymeric nature

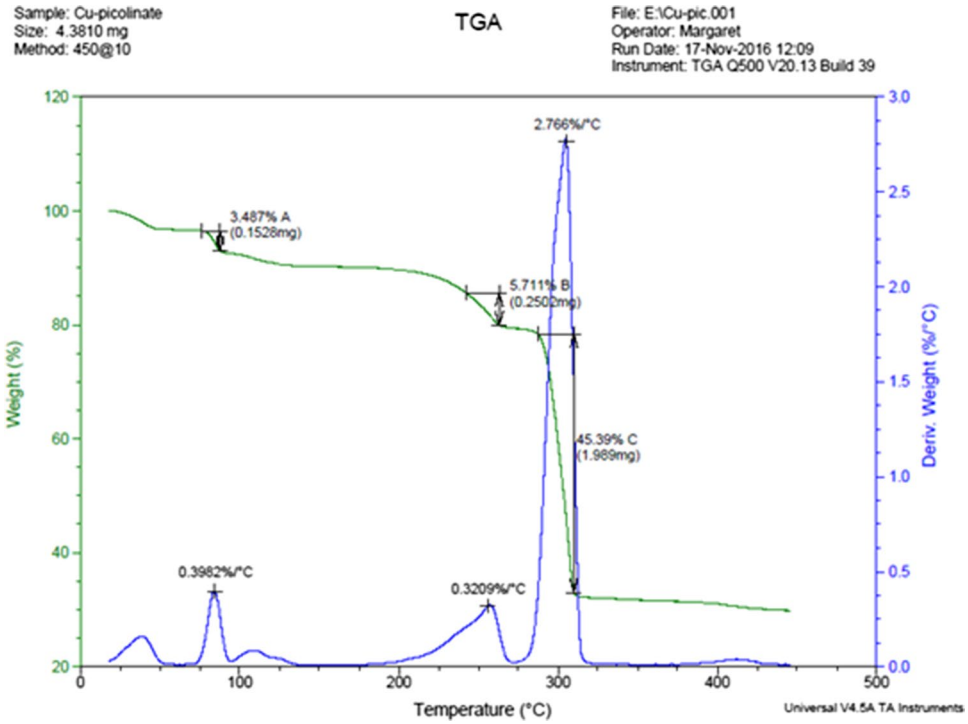

Fig. 5 TGA curve versus temperature gradient of CP-1

up to 25 ppm. Thereafter, an observed decrease occurred since it is toxic at trace amount and higher concentration of pyrene above such concentration causes aggregation of pyrene in solution (Garrett 2004).

This effect is dependent on binding sites of an adsorbent and the PAHs concentration (Jung et al. 2013). Thus, at lower concentrations, there are unoccupied sites still remaining in which the pyrene molecules occupy at higher concentrations.

Effect of contact time

The relationship between contact time and pyrene adsorption (Figure S2) was studied at different time intervals (25 ppm; 25 ± 2 °C; 200 rpm; 4 h; 0.010 g of adsorbent). A rapid removal of pyrene was observed at the beginning before the adsorption process became steady. Optimum time (i.e., the time at which the highest amount of dye adsorbed was obtained) for the adsorption of pyrene over CP-1 was 120 min and later attained equilibrium. The rapid

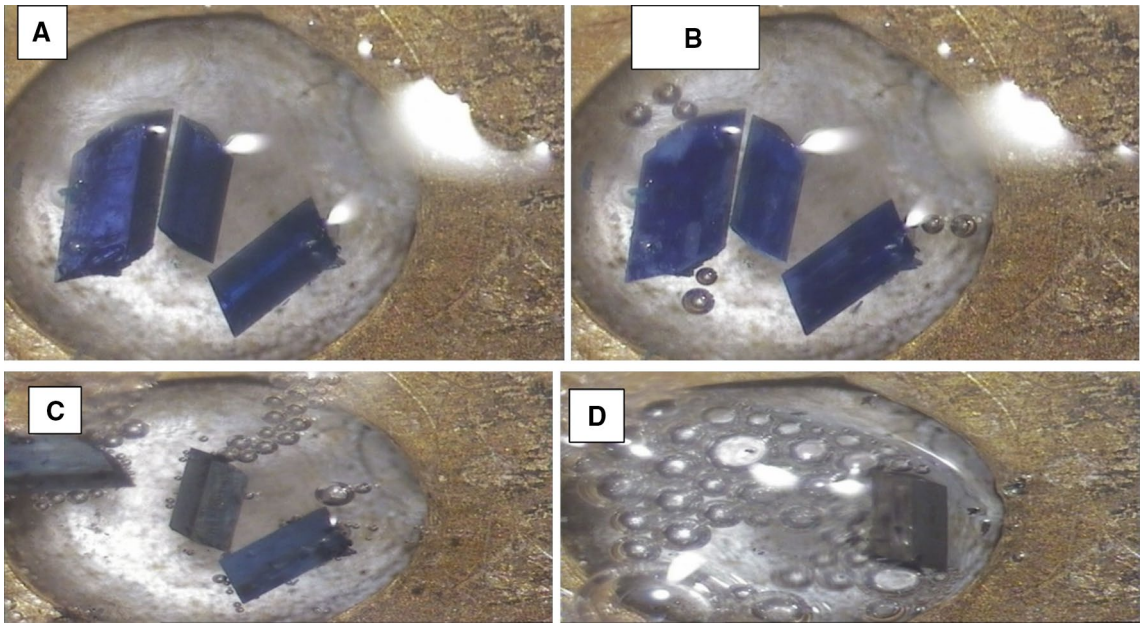

Fig. 6 **a–d** HSM of CP-1

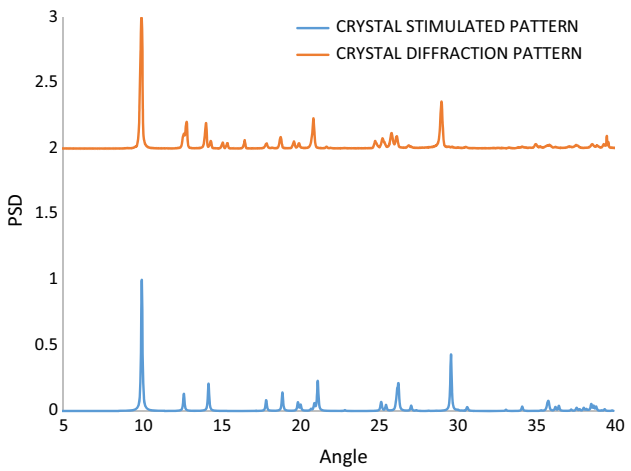

Fig. 7 Superimposition of crystal stimulation and experimental high-resolution diffraction pattern of CP-1

removal observed at the earlier stage may be because of the presence of vacant active sites on the adsorbent which is still unoccupied at the beginning but became occupied by the pyrene molecules as the reaction progressed (Jung et al. 2013).

Effect of temperature

The rate of dependence of the adsorption process on temperature using 0.01 g of adsorbent (Figure S3) showed that the amount of pyrene adsorbed during the adsorption process was reduced as temperature of reaction increased from 25 ± 2 °C to 80 °C (106.48 to 66.89 mg/g).

Effect of adsorbent dosage

A decrease in pyrene uptake was noted, as the adsorbent dose increased (Figure S4), due to the availability of more adsorbent quantity, and thus more sites are available for adsorption of the pyrene molecules which become insufficient to occupy exchangeable sites that present on the 1, resulting in unsaturation of the available sites and low ratio of pyrene uptake to adsorbent dose (Authuner et al. 2001; Amin et al. 2012). The effect of aggregation, at higher concentrations, of the adsorbent molecules can also affect the adsorption process (Authuner et al. 2001; Amin et al. 2012). Also, interference between binding sites due to decreased adsorbent dosages which leads to high specific uptake could account for such pattern as shown in Fig. S4.

Effect of pH

The influence of pH on pyrene adsorption over CP-1 is depicted in Figure S5.

Adsorption of pyrene was found to depend on pH (Singh et al. 2003) for the pyrene adsorption over CP-1, studied for 2 h, at various pH values (2–14). The amount of adsorbed pyrene decreases rapidly with pH increase to pH 6 in the acidic region, which is the minimum pH of adsorption; thereafter, the amount of pyrene adsorbed from the bulk solution increases with pH at the basic region. Lower adsorption capacity in the acidic region may be due to the repulsive effect between adsorbent and pyrene (Jorfi et al. 2013), while the higher adsorption capacity noted at basic pH may be due to conversion of hydrophobic pyrene into 1-hydroxypyrene which is hydrophilic (Hoover 2014). (Pyrene has a major microspecies at pH of 7.4 [34].) Thus, an interaction occurs between the CP-1 [34] and the 1-hydroxypyrene intermediate formed.

Adsorption isotherms of pyrene over CP-1

The adsorption isotherms for CP-1 were deduced after a 2-h adsorption process. The adsorption isotherms were plotted according to the isotherm equations (Temkin, Langmuir, and Dubinin–Radushkevich).

The Q_m and K_L values of the Langmuir for the adsorbent are determined from Figure S6; n and K_f of the Freundlich are also determined from Figure S7; k_T and B_I of Temkin are also determined from Figure S8; and B_D and q_s of Dubinin–Radushkevich are obtained from Figure S9. These values, summarized in Table 4, show the Langmuir model as the most suitable for this pyrene adsorption experiment.

Langmuir isotherm model

The Langmuir isotherm model (Table 4) gave an R^2 value of 0.9415 for pyrene adsorption over CP-1. Maximum adsorption kinetics (Q_m) of CP-1 is high 90.91 with monomolecular capacity of 0.09 at 25 ± 2 °C, meaning that one gram of CP-1 can adsorb 90.91 mg of pyrene. The adsorption processes thus follow Langmuir. This gives an indication that physisorption and chemisorption accompanied with diffusion (intra-particle) are potentially applicable in the adsorptive removal of pyrene.

Freundlich isotherm model

Freundlich model (Table 4) shows the distribution of active centers (exponential), which is the characteristic of heterogeneous surfaces. The values of Freundlich parameters, n and K_f, are 0.73 and 1.56 mg/g for pyrene, indicative of the sorption intensity and capacity, respectively. The $n > 1$ means that sorption capacity is suppressed slightly when at low equilibrium concentration (Hall et al. 1966; Saleem et al. 1992). Alternatively, the value of $n < 1$ is indicative of the increase in binding strength with more attaching sorbates.

The R^2 value of 0.9514 presents the Langmuir model as having the highest value (Figure S6 to S9, and Table 4) for the PAH under study. The isotherms have R^2 values of increasing order 0.941 < 0.893 < 0.8351 < 0.72 corresponding to Dubinin–Radushkevich < Temkin < Freundlich < Langmuir. The favorable and efficient adsorption of pyrene over CP-1 implies the applicability of CP-1 for remediation of pyrene-polluted water. This observation might be due to a very favorable interaction between PAHs and neutral surface of CP-1.

Separation factor

The Langmuir plot was used in calculating the separation factor (R_L). R_L value of 0.95 indicates a favorable adsorption process of pyrene being nearly irreversible as value tends to one (Hall et al. 1966).

$$R_L = (1 + bC_0)^{-1}$$

Adsorption kinetics of pyrene over CP-1

Kinetics of the pyrene sorption process was studied using the first- and second-order equations (Saleem et al. 1992) with data from the influence of contact time on adsorption over CP-1 at a concentration of 25 ppm with various adsorption times (10–240 min). High adsorption capacity noted for CP-1 might be due to favorable interactions of the adsorbate with it. Rapid adsorption occurred at the initial stage premised by amount of vacant sites on the adsorbent (Lee et al. 2007). The adsorption of pyrene over CP-1 was completed after 2 h, and the data subjected to the pseudo-second-order and pseudo-first-order models (Tinge et al. 1987).

Table 4 Isotherm parameters with coefficient of determination (R^2) for the adsorption of pyrene over CP-1 at 25 ± 2 °C

PAH	Langmuir constants		R^2	Freundlich constants		R^2	Temkin constants		R^2	D–R constants		R^2
	Q_m (mg/g)	K_L (L/mg)		K_f (mg/g)	n		b_T (J/mol)	k_T (L/mg)		q_s (mg/g)	E (kJ/mol)	
Pyrene	90.91	0.094	0.9415	1.15	0.73	0.893	7.45	20.094	0.8351	1.46	4×10^{-6}	0.72

Table 5 Pseudo-first-order and pseudo-second-order constants of pyrene

Kinetic model	Rate constant	R^2
Pseudo-second order k_2 (g/mg/min)	3.04×10^{-4}	0.9938
Pseudo-first order k_1 (min^{-1})	97.32	0.9089

Table 6 Weber–Morris parameters of adsorption of pyrene

Parameters	Values
Intra-particle diffusion	
k_I (mg/g min)	10.51
C_I (mg/g)	3.694
R^2	0.9087
k_{II} (mg/g min)	0.6927
C_{II} (mg/g)	09.1155
R^2	0.9669

At equilibrium, 125 mg/g of pyrene was calculated to have been removed by CP-1. The rate constant and correlation coefficient suggest rapid interaction and adsorption of pyrene onto the 3.7.1 CP-1.

The value of k (Table 5) confirms that pyrene adsorption correlates with the second-order model, suggesting that physisorption and chemisorption processes occurred alongside intra-particle diffusion (Table 6).

$$q_t = k_t t^{1/2} + C_i$$

where $t^{1/2}$ is the square root of the time, C_i is the intercept at stage i. Figure S10 presents a typical plot for the adsorption of pyrene on CP-1 using diffusion model.

Figure S11 shows that the plot of q_t versus $t^{1/2}$ shows multilinearity characterizations, indicating that more than one diffusion step takes place. The effect of boundary layer is seen in the curved region of the plot, while the particle diffusion effect is shown by the linear portion. The gradual adsorption is shown by the second depressed portion of the plot, in which intra-particle diffusion slows because of the low level of pyrene remained in solution. The plot from Figure S12 revealed a non-straight line implying the rate-limiting step is controlled by mass transport. Hence, applying the expression (Boyd equation):

$$F = 1 - 6/\pi^2 \exp\left(-B_t\right)$$

$$B = \frac{\pi D}{r^2} = \text{time constant}$$

in which D = diffusion coefficient, r = radius of adsorbent particle, and F = fraction of solute adsorbed at different times, t, and given by:

$$F = \frac{q_t}{q_e}$$

where q_t and q_e = amount adsorbed (mg/g) at any time "t" and infinity "e", respectively, and the kinetic expression becomes

$$B_t = -0.4977 - \ln\left(1 - {}^{q_t}/_{q_e}\right)$$

B_t can obtain using the values of t. Figure S13 shows the calculated B_t values against time for pyrene at 32 ± 2 °C (Figure S13).

The thermodynamics study

Thermodynamic parameters are used to explain the adsorption process.

The pyrene adsorption thermodynamic parameters (such as free energy ΔG, enthalpy ΔH and entropy ΔS) over CP-1 are calculated using the following equations. The ΔG can be calculated with the equation:

$$\Delta G = -RT \ln K_c$$

$$K_c = \frac{C_{\mathrm{Ae}}}{C_{\mathrm{e}}}$$

in which T is the temperature (K) and R is the gas constant (8.314 J/mol/k).

R = gas constant, T = temperature, K_c = equilibrium constant, C_{Ae} = solid phase concentration at equilibrium (mg/L), and C_{e} = equilibrium concentration in solution (mg/L).

The enthalpy (ΔH) and entropy (ΔS) were determined from the van't Hoff equation

$$\ln K_c = (\Delta S)/R - (\Delta H)/RT$$

Plot of $\ln K_c$ versus $1/T$ gave ΔH, which is obtained from the slope ($-$slope $\times R$) of the van't Hoff plot, and (ΔS) from the intercept $\times R$ of the van't Hoff equation (Figure S14).

The values of the thermodynamic parameters for the sorption of PAHs on CP-1 are given in Table 7.

Adsorption capability of 1 decreases with the increase in temperature because mobility of the molecular species increases with temperature (Lee et al. 2007), suggesting that the adsorption of pyrene on CP-1 does not require temperature.

Table 7 Thermodynamic parameters of pyrene adsorption over CP-1

Adsorbate	T (K) $\ln K_c$	ΔG (kJ/mol)	ΔH (kJ/mol)	ΔS (J/mol/K)
Pyrene	298 6.43	− 15.93	− 17.62	5.80
	313 6.07	− 15.79		
	323 5.84	− 15.68		
	333 5.65	− 15.65		
	343 5.45	− 15.60		
	353 5. 31	− 15.59		

The negative ΔG for these processes shown in Table 7 indicate that the highest ΔG (− 15.93 kJ/mol); hence, it becomes negative at higher temperature, suggesting that the process is better favored at lower temperature. The calculated $\Delta H = -17.62$ kJ/mol/K (Table 7) confirms an exothermic process. Physisorption primarily occurs due to van der Waals forces, hydrophobicity, $\pi - \pi$ interactions (Tinge et al. 1987) between the adsorbate and adsorbent.

The entropy value obtained relates to the mobility of molecules within the system, which is the sum of all the sorption processes (adsorption and desorption) occurring in the experiment.

The ΔS value is in agreement with the reported data on increasing entropy when adsorbates adhere to the surface of the adsorbent at an increasing rate. The presence of pyrene molecules on 1 reduces the free movement for the pyrene molecules; thus, a positive value of $\Delta S = 5.80$ suggests an increase in the randomness during the adsorption process and that an affinity existed between CP-1 and pyrene.

The resultant effect of binding and steric hindrance decreases the ΔH value and increases the ΔS for the process (Chauvey et al. 2013; Le Vaillant et al. 2012).

The adsorption of pyrene molecules onto the CP-1 and the desorption of guest molecule from CP-1 are rapid for this experiment. The driving force can thus be proposed as enthalpy effect and not entropy effect (Chauvey et al. 2013).

Adsorption mechanism and characterization of CP-1 after the removal of pyrene

The suggested mechanism could be through the $\pi - \pi$ interaction taking place between the aromatic rings of the pyrene and linker units of CP-1. Similar mechanism was reported by some researchers for adsorption of organic compounds onto coordination polymers (Hassan and Jhung 2015; Pilloni et al. 2015).

The FTIR spectra of CP-1 and CP-1 after adsorption of pyrene were compared, and it was observed that the νC = C ring stretching shifted from 1643 to 1471 cm^{-1} of the CP-1 (before adsorption) to 1598 and 1475 cm^{-1} (after adsorption of pyrene). The νC–H aromatic stretch of 3070 cm^{-1} was still present, but a new band of 2727 cm^{-1} was observed. There was no other major shift in other bands, indicating that the MOF's structure might still be intact as shown in Figure S15.

Reusability studies

The investigation of reusability of CP-1 as an adsorbent was carried out as shown in Fig. 8. CP-1 was used five times for the removal of pyrene. Regeneration experiment was performed by washing the adsorbent with ethanol followed by drying in oven, each time it was used. After being used for five times, the rate of removal decreased by 2.3% (82.4–80.1%). This result suggests that CP-1 has excellent regenerated and reusability capacities.

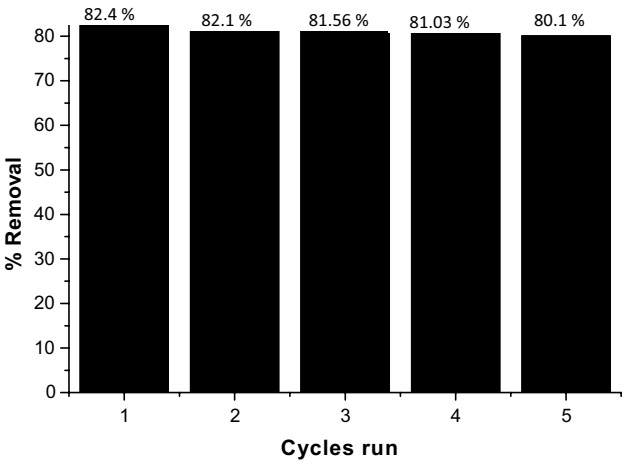

Fig. 8 Reusability test of CP-1 for removal of pyrene

Conclusion

CP-1 was synthesized, characterized and used for adsorptive removal of pyrene. Single X-ray crystal structure of CP-1 displayed octahedral geometric with one water molecule as a guest within the structure of the compound. The Cu^{2+} ion is bonded to four oxygen atoms and two nitrogen atoms of the picolinate ligand. The thermo-gravimetric study and the hot-stage microscope also clearly supported the presence of water molecule within the pore of the polymer backing up the result from X-ray crystallography. Freundlich model shows non-multiple binding site for this adsorption. The thermodynamics reflect the decreased adsorption as temperature rises due to mobility of pyrene molecules which increases, suggesting that the adsorption of an PAH onto CP-1 does not require temperature. The suggested mechanism of adsorption could be through $\pi - \pi$ interaction between CP-1 and pyrene as confirmed from the FTIR. These findings reveal that CP-1 can be an effective adsorbent to remove pyrene from polyaromatic hydrocarbon spillage. In addition, the adsorbent could easily be regenerated and re-used for pyrene adsorption.

Acknowledgements ACT is grateful to Royal Society of Chemistry for the award of 2016 RSC research fund grant. MDO acknowledges financial support from the Organization for Women in Science for the Developing World (OWSD) and the Swedish International Development Cooperation Agency (SIDA).

Compliance with ethical standards

Conflict of interest The authors declare that there is no conflict of interest.

References

Alhamami M, Doan H, Cheng C (2014) A review on breathing behaviors of metal–organic–frameworks (MOFs) for gas adsorption. Materials 7:3198–3250

Ali I, Asim M, Khan TA (2012) Low cost adsorbents for the removal of organic pollutants from wastewater. J Environ Manag 113:170–183

Amin NC, Blanchin MD, Ake M, Fabre H (2012) Capillary electrophoresis for the assay of fixed-dose combination tablets of artesunate and amodiaquine. Malar J 11:149–156

Antolini L, Battaglia LP, Corradi AB, Marcotrigiano G, Menabue L, Pellacani GC, Saladini M (1982) Synthesis, spectroscopic and magnetic properties of mixed-ligand complexes of copper(II) with imidazole and nitrogen-protected amino acids. Inorg Chem 21:1391–1393

Authuner APM, Watkins GM, Duncan JR (2001) Batch studies on the removal of gold (III) from aqueous solution by *Azolla filliculoides*. Biotechnology 23:249–251

Baek SO, Field RA, Goldstone ME, Kirk PW, Lester JN, Perry R (1999) A review of atmospheric polycyclic aromatic hydrocarbons: sources, fate and behavior. Water Air Soil Pollut 60:279–300

Byeong-Kyu L, Van-Tuan V (2010) Sources, distribution and toxicity of polycyclic aromatic hydrocarbons (PAHs) in particulate matter. In: Villanyi V (ed) Air pollution. InTech, Thousand Oaks. https://doi.org/10.5772/10045. ISBN 978-953-307-143-5

Chauvey D, Brenier C, Vaillant YL, Bonnet PA, Nicolas A (2013) Simultaneous determination of Artesunate and Amodiaquine in fixed-dose combination by a rapid and simple reversed phase HPLC method with double UV detection. Biochem Pharmacol 55:843–847

Chen Y, Bi X, Mai B, Sheng G, Fu J (2004) Emission characterization of particulate/gaseous phases and size association for polycyclic aromatic hydrocarbons from residential coal combustion. Fuel 83:781–790

Cooke M, Dennis AJ (eds) (1984) Polynuclear aromatic hydrocarbons: mechanisms, methods and metabolism. Battelle Press, Columbus

Dey C, Kundu T, Biswal BP, Mallick A, Banerjee R (2013) Crystalline metal–organic frameworks (MOFs): synthesis, structure and function. Acta Crystallogr B 70:3–10

Donata L (2011) Polycyclic aromatic hydrocarbons (PAHs) factsheet. JRC 66955, 4th edn. pp 1–34

Garrett CL (2004) Priority substances of interest in the Georgia Basin: profiles and background information on current toxics issues. Report of the Canadian Toxics Work Group, GBAP Publication no. EC/GB/04/79

Hall KR, Eagleton LC, Acrivos A, Vermeulen T (1966) Pore- and solid-diffusion kinetics in fixed-bed adsorption under constant-pattern conditions. Ind Eng Chem Fundam 5(2):212–223

Hassan Z, Jhung SH (2015) Removal of hazardous organics from water using metal–organic frameworks(MOFs): plausible mechanism for selective adsorptions. J Hazard Mater 283:329–339

Hemminki K (1993) DNA adducts, mutations and cancer. Carcinogenesis 14:2007–2012

Hoover R (2014) Need to track organic nano-particles across the universe? NASA's got an App for that. NASA's Ames Research Center. https://www.nasa.gov/ame. Accessed 22 Apr 2018

Jahn H, Teller E (1937) Stability of the polyatomic molecules in degenerate electronic state. I. orbital degeneration. Proc R Soc A 161(905):220–235

Jernelöv A (2010) The threats from oil spills: now, then, and in the future. AMBIO A J Hum Environ 39:1–14

Jorfi S, Rezaee A, Moheb-ali G, Jaafarzadeh NA (2013) Pyrene removal from contaminated soils by modified Fenton oxidation using iron nanoparticles. J Environ Health Sci Eng 11:17

Jung BK, Hasan Z, Jhung SH (2013) Adsorptive removal of 2,4-dichlorophenoxyacetic acid (2,4-D) from water with a metal–organic framework. Chem Eng J 234:99–105

Le Vaillant Y, Brenier C, Grange Y, Nicolas A, Bonnet PA, Massing-Bias LR, Rakotomanga P, Koumaré B, Mahly A, Absi M, Ciss M, Loueslati MH, Chauvey D (2012) Simultaneous determination of artesunate and amodiaquine in fixed-dose combination by a RP-HPLC method with double UV detection: implementation in interlaboratory study involving seven African national quality control laboratories. Chromatographia 75:617–628

Lee SD, Grant L (eds) (1981) Health and ecological assessment of polynuclear aromatic hydrocarbons. Pathotex Publishers, Park Forest South, p 364

Lee CK, Liu SS, Juang LC, Wang CC, Lin KS, Lyu MD (2007) Application of MCM-41 for dyes removal from waste water. J Hazard Mater 147:997–1005

Lee J, Farha OK, Roberts J, Scheidt KA, Nguyen ST, Hupp JT (2009) Metal–organic framework materials as catalysts. Chem Soc Rev 38:1450–1459

Lee YR, Kim J, Ahn WS (2013) Synthesis of metal–organic frameworks: a mini review. Korean J Chem Eng 30(9):1667–1680

Liu WX, Dou H, Wei ZW, Chang B, Qui WX, Liu Y, Shu T (2008) Emission characteristics of polycyclic aromatic hydrocarbons from combustion of different residential coals in North China. Sci Total Environ 407:1436–1446

Mueller U, Schubert M, Teich F, Puetter H, Schierle-Arndt K, Pastré J (2006) Metal–organic frameworks—prospective industrial applications. J Mater Chem 16:626–636

Nriagu JO (2011) Oil industry and the health of communities in the Niger Delta of Nigeria. Encycl Environ Health 4:558–567

Pilloni M, Padella F, Ennas G, Lai S, Bellusci M, Rombi E, Sini F, Pentimalli M, Delitala C, Scano A, Cabras V, Ferino I (2015) Liquid-assisted mechanochemical synthesis of an iron carboxylate metal–organic framework and its evaluation in diesel fuel desulfurization. Microporous Mesoporous Mater 213:14–21

Ravindra K, Bencs L, Wauters E, de Hoog J, Deutsch F, Roekens E, Bleux N, Bergmans P, Van Grieken R (2006) Seasonal and site specific variation in vapor and aerosol phase PAHs over Flanders (Belgium) and their relation with anthropogenic activities. Atmos Environ 40:771–785

Saleem M, Afzal M, Qadeer R, Hanif J (1992) Selective adsorption of uranium on activated-charcoal from electrolytic aqueous solutions. Sep Sci Technol 27(2):239–253

Schlichte K, Kratzke T, Kaskel S (2004) H_2 and CH_4 Sorption on Cu-BTC metal organic frameworks at pressures up to 15 MPa and temperatures between 273 and 318 K. Microporous Mesoporous Mater 73(1–2):81–88

Shriver DF, Atkins PW (1999) Inorganic chemistry, 3rd edn. Oxford University, Oxford, pp 235–236

Singh KP, Mohan D, Sinha S, Tondon GS, Gosh D (2003) Color removal from wastewater using low activated carbon derived from agricultural waste material. Ind Eng Chem Res 42:1965–1976

Tella AC, Aaron IY (2012) Syntheses and applications of metal–organic frameworks materials: a review. Acta Chim Pharm Indica 2(2):75–81

Tella AC, Owalude SO, Ojekanmi CA, Oluwafemi OS (2014) Synthesis of copper–isonicotinate metal–organic frameworks simply by mixing solid reactants and investigation of their adsorptive properties for the removal of the fluorescein dye. New J Chem 38:4494–4500

Tella AC, Olawale MD, Neuburger M, Obaleye JA (2017a) Synthesis and crystal structure of Cd-based metal–organic framework for removal of methyl-orange from aqueous solution. J Solid State Chem 255:157–166

Tella AC, Owalude SO, Olatunji SJ, Adimula VO, Elaigwu SE, Alimi LO, Ajibade PA, Oluwafemi OS (2017b) Synthesis of zinc-carboxylate metal–organic frameworks for the removal of emerging drug contaminant (amodiaquine) from aqueous solution. J Environ Sci 64:264–275

Tella AC, Owalude SO, Olatunji SJ, Oloyede SO, Ogunlaja AS, Bourne SA (2018) Synthesis, crystal structure and desulfurization properties of zig–zag 1D coordination polymer of copper(II) containing 4-methoxybenzoic acid ligand. J Sulfur Chem 39(6):588–606

Tinge JT, Mencke K, Drinkenburg AAH (1987) The adsorption of propane and ethane in slurries of activated carbon in water-I. Chem Eng Sci 42:1899–1907

Zhao Y, Song Z, Li X, Sun Q, Cheng N, Lawes S, Sun X (2016) Metal–organic frameworks for energy storage and conversion. Energy Stor Mater 2:35–62

Zhu L, Lu H, Chen S, Amagai T (2009) Pollution level, phase distribution and source analysis of polycyclic aromatic hydrocarbons in residential air in Hangzhou. China J Hazard Mater 162:1165–1170